Affine Parameter-Dependent Preview Control for Rotorcraft Terrain Following Flight

Nuno Paulino [*], Carlos Silvestre [†] and Rita Cunha [‡]

Instituto Superior Técnico, Institute for Systems and Robotics, 1049-001 Lisbon, Portugal

This paper presents a terrain following controller for rotorcraft that takes into account the terrain characteristics ahead of the vehicle as measured by a Laser Range Scanner. The methodology used to solve the terrain following control problem amounts to posing it as a discrete time path following control problem where a conveniently defined error state space model of the plant is augmented with terrain preview data. A piecewise affine parameter-dependent model representation is used to accurately describe the linearized error dynamics for a pre-defined set of operating regions. For each region, the synthesis problem is stated as a state feedback H_2 control problem for affine parameter-dependent systems and solved using Linear Matrix Inequalities (LMIs). An alternative technique to compute the feed-forward preview gain matrix is proposed that avoids solving LMIs involving a large number of unknowns. The resulting nonlinear controller is implemented within the scope of gain-scheduled control theory using the D-methodology. Simulation results obtained with the full nonlinear helicopter model are presented and discussed.

I. Introduction

Recent advances in sensor technology and the increasing availability of computational capacity are steadily affording Unmanned Air Vehicles (UAVs) higher degrees of robustness and reliability in challenging and uncertain operation scenarios. Model-scale helicopters constitute one of the most versatile and cost-effective UAV platforms with a wide and valuable range of applications, such as crop spraying, fire surveillance, and bridge and building inspection. Unlike fixed-wing aircraft, helicopters were designed to execute vertical flight maneuvers, including hovering and vertical take-off and landing (VTOL). Moreover, their ability to perform agile maneuvers both at high and low speeds does not undermine the good flying qualities displayed in fast

[*]MSc Student, Department of Electrical Engineering and Computer Science, Av. Rovisco Pais 1; paulino@isr.ist.utl.pt.

[†]Assistant Professor, Department of Electrical Engineering and Computer Science, Av. Rovisco Pais 1; cjs@isr.ist.utl.pt. Member AIAA.

[‡]PhD Student, Department of Electrical Engineering and Computer Science, Av. Rovisco Pais 1; rita@isr.ist.utl.pt.

forward flight. The trade-off for such maneuverability is an inherent complexity that translates into a highly nonlinear and unstable dynamical system with wide parameter variations over the vehicle's flight envelope. In this context, the development of terrain following control systems constitutes both a challenge and a fundamental requirement for accomplishing of high performance low altitude autonomous flight.

This paper presents a terrain following controller, based on a novel preview control algorithm. Preview control algorithms have been widely used to improve the overall closed loop performance obtained with limited bandwidth feedback compensators when future information on the commands or disturbances is available. A series of papers on application of the Linear Quadratic preview control theory to the design of vehicle active suspensions can be found in the literature. Special emphasis should be given to the pioneering work of Tomizuka,[1] where the optimal preview control problem is formulated and solved, and the impact of different preview lengths on the overall suspension performance is discussed. An alternative method is presented by Prokop and Sharp[2] that consists of incorporating the disturbance or reference dynamics into the design model and then solving the resulting linear quadratic control problem. More recently, Takaba[3] addressed the problem of a robust servomechanism with preview action mixed LQ/H_∞ design for polytopic uncertain systems using Linear Matrix Inequalities.

Related work in the area with applications to helicopters can be found in Ref. 4, where authors apply the Generalized Predictive Control (GPC) algorithm to a rotorcraft terrain-following problem. In this work, the performance of the resultant controller is compared to that of a conventional compensator in terms of flight path following, control activity, and control law implementation.

For linear control systems design, the paper exploits the use of a discrete time state feedback H_2 preview control problem for affine parameter-dependent systems. Much of the work in this area is well rooted in the theory of Linear Matrix Inequalities (LMIs), which are steadily becoming a standard tool for advanced control system design. In fact, many control problems can be cast as LMI problems that can be solved efficiently using convex programming techniques. In the approach pursued in this paper, results presented in Refs. 3, 5, 6 were used to develop the LMI based H_2 preview controller synthesis algorithm for affine parameter-dependent systems. For large preview intervals the technique proposed in the paper leads to LMI optimization problems involving a large number of variables. To tackle this problem, an alternative algorithm for computing the feedforward gain matrix is proposed, one which exploits the particular structure of the augmented preview system.

In the paper, linear state feedback preview controllers are synthesized for a finite number of piecewise affine parameter-dependent discrete time plant models. Each of these models consists of the discrete equivalent of the generalized error linearization for each of the helicopter operating regions determined by a well-defined box in the parameter space (vehicle's total speed and angle of attack). The adopted error space is in line with the solutions presented in Refs. 7–9 and exhibits high directionality accuracy, by taking into account the current vehicle orientation in the definition of the reference velocities.

The resulting controllers are then switched as function of the scheduling variables that parameterize the helicopter operating regions. The final implementation of the non-linear gain scheduled controller is obtained using the D-methodology presented in Ref. 10, which guarantees a fundamental linearization property and avoids the need to feedforward the values of the state variables and inputs at trimming.

A key question underlying the design of sensor based terrain following control systems is computation of the terrain elevation data from sensor measurements. In this paper, the technique adopted exploits the sensor geometry to efficiently build the terrain profile ahead of the vehicle.

The controller design and performance evaluation of the overall closed loop system relies on an accurate self-contained helicopter dynamic model, derived from first-principles, that is specially tailored for model-scale helicopters.[11] The simulation model, implemented in Matlab, using Simulink and CMEX-file S-functions, includes rigid body, main rotor flapping, and Bell-Hiller stabilizing bar dynamics and is parameterized for the case of the Vario X-Treme acrobatic helicopter.

The paper is organized as follows. In Section II, a nonlinear dynamic model for model-scale helicopters is presented. Section III introduces the path-dependent error space used to describe the vehicle dynamics. Section IV states the preview control problem. Section V describes the methodology adopted for H_2 linear controller design where an LMI synthesis technique is applied to affine parameter-dependent systems. Section VI presents the reconstruction technique used to build the reference path from Laser Range Scanner measurements. Section VII focuses on implementation of the nonlinear terrain following controller for the Vario X-treme helicopter. Finally, simulation results obtained with the full nonlinear dynamic model are presented in Section VIII.

II. Helicopter dynamic model

Figure 1. ***Vario X-treme*** **model-scale helicopter.**

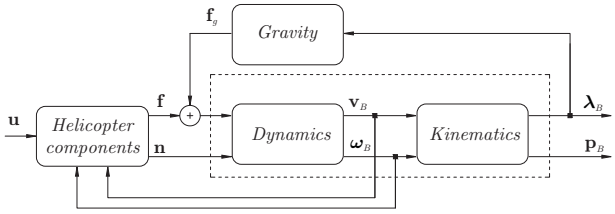

Figure 2. Block diagram of the non-linear model.

The helicopter dynamic model presented here was the basis for development of a simulator, named *SimModHeli*,[11] implemented in Matlab, using Simulink and C MEX-file S-functions, which is freely available to the scientific community. This simulator is completely parameterizable and describes the dynamics of helicopters with any number of blades, with or without a Hiller or Bell-Hiller stabilizing bar. The simulation model is specially tailored for model-scale helicopters, such as the one depicted in Figure 1. In this paper, for

controller design purposes, a simplified model adequate for low speed flight regimes is adopted. The analysis leading to this simplified model is discussed in Ref. 11.

The helicopter dynamics are described using a conventional six degree of freedom rigid body model driven by forces and moments that explicitly include the effects of the main rotor, Bell-Hiller stabilizing bar, tail rotor, fuselage, horizontal tailplane, and vertical fin. The main rotor is the primary source of lift and propulsion, generating forces and moments that enable control of the aircraft position, orientation and velocity. The Bell-Hiller stabilizing bar improves the stability characteristics of the helicopter. The tail rotor, located at the tail boom, provides the moment needed to counteract the torque generated by the aerodynamic drag forces at the rotor hub. The remaining components have less significant contributions and can be described by simpler models. In short, the fuselage produces drag forces and moments and the horizontal tailplane and vertical fin act as wings in forward flight, increasing flight efficiency. A detailed description of the helicopter dynamic model can be found in Ref. 11.

The equations of motion were derived using the following notation:

$\{I\}$ - inertial coordinate frame;

$\{B\}$ - body-fixed coordinate frame, with origin at the vehicle's center of mass;

$\mathbf{p}_B = [x, y, z]^T$ - position of the vehicle's center of mass, expressed in $\{I\}$;

$\boldsymbol{\lambda}_B = [\phi_B, \theta_B, \psi_B]^T$ - *Z-Y-X* Euler angles that locally parameterize the orientation of the vehicle relative to $\{I\}$;

$\mathbf{v}_B = [u, v, w]^T$ - body-fixed linear velocity vector;

$\boldsymbol{\omega}_B = [p, q, r]^T$ - body-fixed angular velocity vector.

Figure 2 captures the general structure of a rigid-body helicopter model, which can be written as

$$\begin{cases} m\dot{\mathbf{v}}_B &= \mathbf{f}(\mathbf{v}_B, \boldsymbol{\omega}_B, \mathbf{u}) + m\, {}^B_I\mathcal{R}\,[0\ 0\ g]^T - \mathcal{S}(\boldsymbol{\omega}_B)\, m\mathbf{v}_B \\ I_B\dot{\boldsymbol{\omega}}_B &= \mathbf{n}(\mathbf{v}_B, \boldsymbol{\omega}_B, \mathbf{u}) - \mathcal{S}(\boldsymbol{\omega}_B)\, I_B\boldsymbol{\omega}_B \\ \dot{\mathbf{p}}_B &= {}^I_B\mathcal{R}\,\mathbf{v}_B \\ \dot{\boldsymbol{\lambda}}_B &= \mathcal{Q}(\phi_B, \theta_B)\,\boldsymbol{\omega}_B, \end{cases} \tag{1}$$

where m is the vehicle's mass, I_B is the tensor of inertia about the $\{B\}$ frame, $\mathbf{f}$ and $\mathbf{n}$ are the vectors of external forces and moments respectively, g is the gravitational acceleration, ${}^B_I\mathcal{R}$ is the rotation matrix from $\{I\}$ to $\{B\}$, $\mathcal{S}(\mathbf{x})$ is a skew-symmetric matrix, defined such that $\mathcal{S}(\mathbf{x})\,\mathbf{y} = \mathbf{x} \times \mathbf{y}$, and $\mathcal{Q}(\phi_B, \theta_B)$ is the transformation from angular speeds to Euler angle derivatives given by

$$\mathcal{Q}(\phi_B, \theta_B) = \begin{bmatrix} 1 & \sin\phi_B \tan\theta_B & \cos\phi_B \tan\theta_B \\ 0 & \cos\phi_B & -\sin\phi_B \\ 0 & \sin\phi_B/\cos\theta_B & \cos\phi_B/\cos\theta_B \end{bmatrix}.$$

The external force and moment vectors are functions of the vehicle velocities and of the command vector $\mathbf{u} = [\delta_0, \delta_{1c}, \delta_{1s}, \delta_{0t}]^T$, which consists of the main rotor collective input δ_0, main rotor and flybar cyclic inputs δ_{1c} and δ_{1s}, and tail rotor collective input δ_{0t}.

III. Error Space

The problem of steering the vehicle along a predefined path, which ultimately allows for definition of a terrain following controller, can be converted into a regulation problem by expressing the state of the vehicle in a conveniently defined error space. This definition requires the introduction of two coordinate systems: the Serret-Frenet frame, $\{T\}$, with origin at the point on the path closest to the vehicle and coordinate axes corresponding to the tangent, normal, and binormal vectors defined at that point; and the desired body frame, $\{C\}$, which defines the reference for orientation at each point on the path. References for the tangent

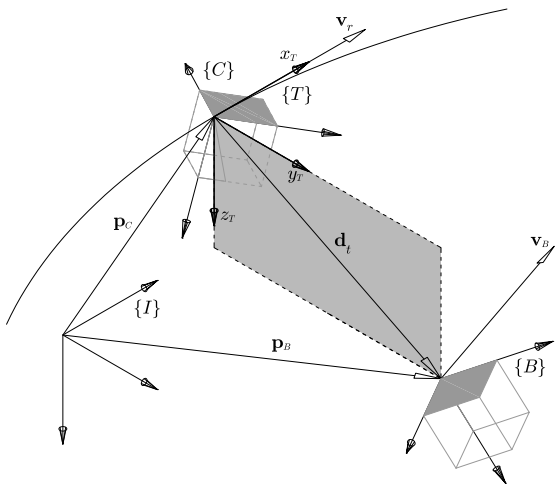

Figure 3. Coordinate frames: Inertial $\{I\}$; Body $\{B\}$; Serret Frenet $\{T\}$; Desired body $\{C\}$.

velocities are also required, with $\mathbf{v}_r = [V_r\ 0\ 0]^T$ denoting the desired linear velocity and $\boldsymbol{\omega}_r$ the desired angular velocity.

Given these definitions, and according to Ref. 7, an error state vector $\mathbf{x}_e \in \mathbb{R}^{11}$ and output $\mathbf{y}_e \in \mathbb{R}^4$ can be introduced

$$\mathbf{x}_e = \begin{bmatrix} \mathbf{v}_e \\ \boldsymbol{\omega}_e \\ \mathbf{d}_t \\ \boldsymbol{\lambda}_e \end{bmatrix} = \begin{bmatrix} \mathbf{v}_B - {}^B_T\mathcal{R}\,\mathbf{v}_r \\ \boldsymbol{\omega}_B - {}^B_T\mathcal{R}\,\boldsymbol{\omega}_r \\ \Pi_{yz}\ {}^T_I\mathcal{R}\,(\mathbf{p}_B - \mathbf{p}_C) \\ \boldsymbol{\lambda}_B - \boldsymbol{\lambda}_C \end{bmatrix} \tag{2}$$

and

$$\mathbf{y}_e = \begin{bmatrix} \mathbf{v}_e + \ {}^{B}_{T}\mathcal{R}\,[0\ \mathbf{d}_t^T]^T \\ \psi_e \end{bmatrix}, \tag{3}$$

where $\Pi_{yz} = \begin{bmatrix} 0 & 1 & 0 \\ 0 & 0 & 1 \end{bmatrix}$, the vectors $\mathbf{p}_B$ and $\mathbf{p}_C$ are the origins of $\{B\}$ and $\{C\}$ expressed in $\{I\}$, and $\boldsymbol{\lambda}_C$ is the vector of Euler angles representing the orientation of $\{C\}$ with respect to $\{I\}$. It is straightforward to verify that the vehicle follows the path with tangent velocities $\mathbf{v}_r$ and $\boldsymbol{\omega}_r$ and orientation $\boldsymbol{\lambda}_C$ if and only if $\mathbf{x}_e = 0$.

The output vector $\mathbf{y}_e$ corresponds to a combination of error vector components expressed on the body coordinate system, which is added for tracking purposes. By including $\mathbf{v}_e$ and $\mathbf{d}_t$ in $\mathbf{y}_e$, both the velocity and position errors are being considered, with the distance vector expressed in the current body frame. The choice of ψ_e as the remaining output arises from the specific characteristics of the helicopter. It can be shown that a helicopter may describe a trimming trajectory, with arbitrary but constant yaw angle relative to the path being followed, automatically constraining the roll and pitch angles.

Assuming that the reference path satisfies $\boldsymbol{\omega}_r = 0$, $\dot{\boldsymbol{\lambda}}_C = 0$, the error dynamics can be written as

$$\begin{cases} \dot{\mathbf{v}}_e &= \dot{\mathbf{v}}_B + \ \mathcal{S}\left(\boldsymbol{\omega}_e\right)\ {}^{B}_{T}\mathcal{R}\,\mathbf{v}_r - \ {}^{B}_{I}\mathcal{R}\,\frac{d}{dt}\left(\ {}^{I}_{T}\mathcal{R}\,\mathbf{v}_r\right) \\ \dot{\boldsymbol{\omega}}_e &= \dot{\boldsymbol{\omega}}_B \\ \dot{\mathbf{d}}_t &= \Pi_{yz}\ {}^{T}_{B}\mathcal{R}\,\mathbf{v}_e - \Pi_{yz}\ \mathcal{S}\left(\boldsymbol{\omega}_T\right) \begin{bmatrix} 0 \\ \mathbf{d}_t \end{bmatrix} \\ \dot{\boldsymbol{\lambda}}_e &= \mathcal{Q}(\phi_e + \phi_C, \theta_e + \theta_C)\boldsymbol{\omega}_e \end{cases}, \tag{4}$$

where $\boldsymbol{\omega}_T = \ {}^{T}_{I}\mathcal{R}\,{}^{I}\boldsymbol{\omega}_T$ is the angular velocity of $\{T\}$ relative to $\{I\}$ expressed in $\{T\}$. Further details on the derivation of the error dynamics can be found in Ref. 7.

A. Error linearization and discretization

For a given straight line path ($\boldsymbol{\omega}_T = 0$), linear speed V_r, and orientation $\boldsymbol{\lambda}_C$, define $\mathbf{u}_c$ as the constant input vector that satisfies (1) at equilibrium ($\dot{\mathbf{v}}_B = 0$, $\dot{\boldsymbol{\omega}}_B = 0$), with $\mathbf{v}_B = \ {}^{C}_{T}\mathcal{R}\,\mathbf{v}_r$, $\boldsymbol{\omega}_B = 0$, and $\boldsymbol{\lambda}_B = \boldsymbol{\lambda}_C$. Then, the linearization of (4) with output vector $\mathbf{y}_e$ about the equilibrium point $\mathbf{x}_e = 0$, $\mathbf{u} = \mathbf{u}_c$ results in

$$\delta\dot{\mathbf{x}}_e = A_e\delta\mathbf{x}_e + B_e\delta\mathbf{u}, \tag{5}$$

$$\delta\mathbf{y}_e = C_e\delta\mathbf{x}_e, \tag{6}$$

where A_e, B_e, and C_e denote the Jacobians evaluated at the equilibrium condition.

The discrete time equivalent of the linear continuous time model (5) is obtained using the zero-order hold on the inputs technique. Let T be the sampling time and define, with obvious abuse of notation,

the augmented discrete time state $\mathbf{x}_d(k) = [\mathbf{x}_e(k)^T, \mathbf{x}_i(k)^T]^T$, where $\mathbf{x}_i(k)$ corresponds to the discrete time integral of $\mathbf{y}_e$. Using this notation, the discrete error dynamics can be written as

$$\mathbf{x}_d(k+1) = A\mathbf{x}_d(k) + B\mathbf{u}(k), \tag{7}$$

where $A = \begin{bmatrix} e^{A_e T} & 0 \\ C_e & I \end{bmatrix}$ and $B = \begin{bmatrix} \int_0^T e^{A_e \tau} d\tau B_e \\ 0 \end{bmatrix}$.

IV. Preview Problem Formulation

Better terrain following performance with limited bandwidth compensators can be achieved by taking into account, in the control law, the terrain characteristics ahead of the helicopter obtained from measurements of a forward looking laser range scanner. The technique used in this paper to develop a tracking controller generalizes the results presented in Ref. 12, and amounts to augmenting the discrete time error space dynamics with a description of the future terrain evolution as seen by the platform.

With the objective of including future path disturbances in the discrete time error space dynamics (7), assume that the helicopter moves with constant speed and attitude along a given reference path that results from the concatenation of straight lines. A detailed analysis of the error dynamics (4) suggests the introduction of the term ${}^I\dot{\mathbf{v}}_r = \frac{d}{dt}\left({}^I_T\mathcal{R}\, \mathbf{v}_r \right)$ as the perturbation to be previewed. Using this interpretation, the disturbance signal, as seen from the helicopter, can be modeled as ${}^I\dot{\mathbf{v}}_r(t) = \sum_i \mathbf{s}(t_i)\delta(t - t_i)$, where $\mathbf{s}(t_i)$ represents an intensity vector, $\delta(t - t_i)$ is the Dirac's delta function, and t_i corresponds to the *ith* concatenation point crossing time. From (5) the resulting linear error dynamics can be written as

$$\begin{aligned} \delta\dot{\mathbf{x}}_e &= A_e\delta\mathbf{x}_e + B_e\delta\mathbf{u} + W\delta^I\dot{\mathbf{v}}_r, \\ W &= [-\, {}^C_I\mathcal{R}^{\,T}\, 0]^T, \end{aligned} \tag{8}$$

and the corresponding discretization is given by

$$\mathbf{x}_d(k+1) = A\mathbf{x}_d(k) + B\mathbf{u}(k) + B_1\mathbf{s}(k), \tag{9}$$

where $B_1 = [(e^{A_e T}W)^T, 0]^T$ is obtained from the impulse invariant discrete equivalent of the injection matrix W. It is assumed that the sampling period is sufficiently small to consider the reference path changes synchronized with the sampling time. Once again with obvious abuse of notation, $\mathbf{s}(k) \in \mathbb{R}^s$ corresponds to

$$\mathbf{s}(k) = {}^I\mathbf{v}_r(k+1) - {}^I\mathbf{v}_r(k). \tag{10}$$

Assuming a preview length of p samples, let $\mathbf{x}_s(k) = [\mathbf{s}(k)^T, \mathbf{s}(k+1)^T, ..., \mathbf{s}(k+p)^T]^T \in \mathbb{R}^{(s(p+1))\times 1}$ be the vector containing all the preview inputs at instant k. The discrete time dynamics of vector $\mathbf{x}_s(k)$ can be modeled as a FIFO queue, given by

$$\mathbf{x}_s(k+1) = D\mathbf{x}_s(k) + B_s\mathbf{s}(k+p+1), \tag{11}$$

where

$$D = \begin{bmatrix} 0 & I & 0 & \cdots & 0 \\ 0 & 0 & I & \cdots & 0 \\ \vdots & \vdots & \ddots & \ddots & \vdots \\ 0 & 0 & 0 & \ddots & I \\ 0 & 0 & 0 & \cdots & 0 \end{bmatrix}, \quad B_s = \begin{bmatrix} 0 \\ 0 \\ \vdots \\ I \end{bmatrix}.$$

Combining the dynamic representation of the terrain (11) with (9) yields the augmented system

$$\mathbf{x}(k+1) = \bar{A}\mathbf{x}(k) + \bar{B}_s\mathbf{s}(k) + \bar{B}\mathbf{u}(k), \tag{12}$$

where

$$\mathbf{x}(k) = \begin{bmatrix} \mathbf{x}_d(k) \\ \mathbf{x}_s(k) \end{bmatrix}, \quad \bar{A} = \begin{bmatrix} A & H \\ 0 & D \end{bmatrix}, \quad \bar{B}_s = \begin{bmatrix} 0 \\ B_s \end{bmatrix}, \quad \bar{B} = \begin{bmatrix} B \\ 0 \end{bmatrix},$$

and $H = [B_1, 0, 0, \cdots, 0]$ represents the injection matrix of the preview signals into the error dynamics. Notice that the D matrix is stable and therefore the augmented system (12) preserves the stabilizability and detectability properties of the original plant.

With the present technique, the preview information is retrieved at p points selected along the path, equally spaced by the distance $d_p = V_t(k)T$. The scalar $V_t(k)$ corresponds to the norm of the projection of the vehicle's velocity vector $\mathbf{v}_B$ on the path, computed at instant k, which can be obtained from $V_t = [1\ 0\ 0]\ {}^T_B\mathcal{R}\,\mathbf{v}_B$. This fact turns out to be of utmost importance, since it allows to naturally redefine the controller visibility distance as a function of the vehicle's speed, preserving the size of the preview input vector. An example of this property is shown in Figure 4, where path preview vectors were obtained for two different speeds. From the figure, it becomes clear how the vehicle velocity has an impact on the visibility distance. The limit case $\mathbf{v}_B \to 0$ results in a pure hovering maneuver where the preview samples are taken from a fixed point on the path.

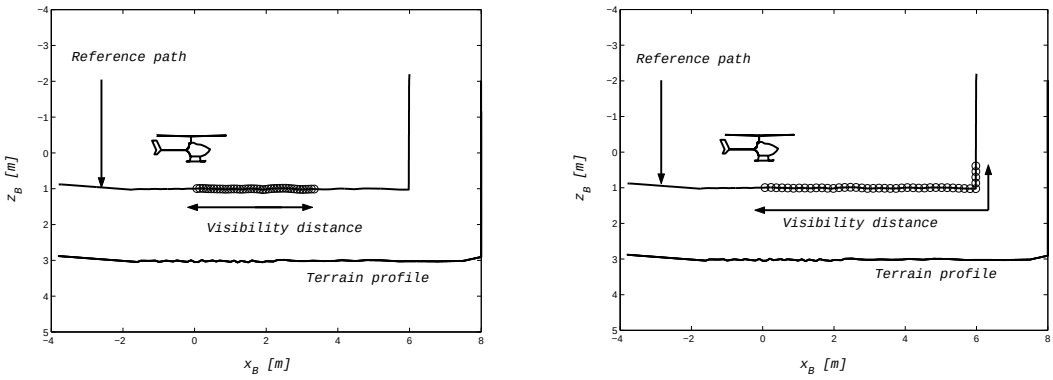

(a) $V_t = 4\,\mathrm{ms}^{-1}$ (b) $V_t = 8\,\mathrm{ms}^{-1}$

Figure 4. Representation of 40 preview samples over the reference path for different speeds.

V. Discrete Time Controller Design

This section presents a solution for the discrete time state feedback H_2 preview control problem for affine parameter-dependent systems. In the approach pursued in this paper, results presented in Ref. 3, 5, 6 were used to develop the LMI based controller synthesis algorithm. Much of the work in this area is well rooted in the theory of LMIs, which are steadily becoming a standard tool for advanced control system design. In fact, LMIs provide a powerful formulation framework as well as a versatile design technique for a wide variety of linear control problems. Since solving LMIs is a convex optimization problem for which numerical solvers are now available, an LMI based formulation can be seen as a practical solution for many control problems.

A. Theoretical background

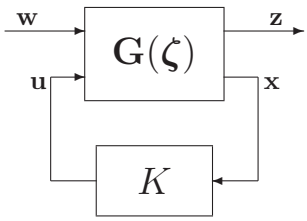

Figure 5. Feedback interconnection.

In what follows, the standard set-up and nomenclature used in Ref. 13 is adopted, leading to the state-space LFT feedback system represented in Figure 5. Consider the generalized affine parameter-dependent system $\mathbf{G}(\boldsymbol{\zeta})$ as a function of the slowly varying parameter vector $\boldsymbol{\zeta}$. It is assumed that $\boldsymbol{\zeta}$ is in a compact set $\Theta \in \mathbb{R}^q$. Suppose that the parameter set Θ can be partitioned into a family of regions that are compact closed subsets Θ_i, $i = 1, \ldots, N$ and that cover the desired helicopter flight envelope. In the ith parameter region $\boldsymbol{\zeta} \in \Theta_i$ the dynamic behavior of the closed-loop system satisfies the realization

$$\left\{ \begin{array}{rcl} \mathbf{x}(k+1) & = & A(\boldsymbol{\zeta})\mathbf{x}(k) + B_w(\boldsymbol{\zeta})\mathbf{w}(k) + B(\boldsymbol{\zeta})\mathbf{u}(k) \\ \mathbf{z}(k) & = & C_z(\boldsymbol{\zeta})\mathbf{x}(k) + E(\boldsymbol{\zeta})\mathbf{u}(k) \end{array} \right. , \quad \mathbf{u}(k) = K\mathbf{x}(k), \tag{13}$$

where $\mathbf{x}(k)$ is the state vector. The symbol $\mathbf{w}(k)$ denotes the input vector of exogenous signals (including commands, disturbances and preview signals), $\mathbf{z}(k)$ is the output vector of errors to be reduced during the controller design process, and $\mathbf{u}(k)$ is the vector of actuation signals. Matrices $A(\boldsymbol{\zeta})$, $B_w(\boldsymbol{\zeta})$, $B(\boldsymbol{\zeta})$, $C_z(\boldsymbol{\zeta})$, and $E(\boldsymbol{\zeta})$ are affine functions of the parameter vector $\boldsymbol{\zeta} = [\zeta_1, \ldots, \zeta_q]^T$, e.g. $A(\boldsymbol{\zeta}) = A^{(0)} + \zeta_1 A^{(1)} + \ldots + \zeta_q A^{(q)}$. The generalized affine parameter-dependent system $\mathrm{G}(\boldsymbol{\zeta})$ consists of the plant to be controlled, together with appended weights that shape the exogenous and internal signals and the preview dynamics presented in Section IV.

For a given parameter region $\Delta \equiv \Theta_i$, assume that the elements that constitute the parameter vector $\boldsymbol{\zeta}$ have their values confined to the interval $\zeta_j \in [\underline{\zeta}_j, \overline{\zeta}_j]$, $\overline{\zeta}_j \geq \underline{\zeta}_j$, $j = 1, \ldots, q$ and define Δ_0 as the set of the

$m = 2^q$ vertices of the parameter-dependent region

$$\Delta_0 \quad := \quad \{\boldsymbol{\zeta} = [\zeta_1, \ldots, \zeta_q]^T : \zeta_j \in \{\underline{\zeta}_j, \overline{\zeta}_j\},\, j = 1, \ldots, q\}.$$

Then Δ corresponds to the convex hull of Δ_0, $\Delta = co\{\Delta_0\}$, which is the smallest convex set containing all the points in Δ_0. The following result, which can be found in Ref. 5, is fundamental for affine parameter dependent systems.

Result 1. *Let $f : \Delta \to \mathbb{R}$ be a convex function where $\Delta = co\{\Delta_0\}$. Then $f(\boldsymbol{\zeta}) \leq \gamma,\ \forall\ \boldsymbol{\zeta} \in \Delta$, if and only if $f(\boldsymbol{\zeta}) \leq \gamma,\ \forall\ \boldsymbol{\zeta} \in \Delta_0$.*

Suppose that the feedback system is well-posed, and let $\mathrm{T}_{\mathbf{zw}}$ denote the closed loop operator from $\mathbf{w}$ to $\mathbf{z}$. The discrete time state feedback H_2 synthesis problem consists of finding (if it exists) a static controller K that stabilizes the closed loop system and makes the H_2 norm $\|\mathrm{T}_{\mathbf{zw}}\|_2$ of the operator $\mathrm{T}_{\mathbf{zw}}$ smaller than a desired bound $\gamma > 0$. The technique used for controller design relies on results available in Ref. 5 and Ref. 14, the most important of which are summarized below after being rewritten for the case of affine parameter-dependent systems. In the following, $\mathrm{tr}(L)$, $\mathrm{im}(L)$, and $\ker(L)$ denote the trace, image, and kernel of matrix L, respectively, and A_i, B_i, C_{z_i}, E_i and B_{w_i} represent the state space matrices of (13) for the $i = 1, \ldots, m$ points in Δ_0.

Result 2. *A static state feedback controller guarantees the γ upper-bound for the discrete time H_2 norm of the closed loop operator $\mathrm{T}_{\mathbf{zw}}(\boldsymbol{\zeta})$ with $\boldsymbol{\zeta} \in \Delta$, that is*

$$\|\mathrm{T}_{\mathbf{zw}}(\boldsymbol{\zeta})\|_2 = \|(C_z(\boldsymbol{\zeta}) + E(\boldsymbol{\zeta})K)\big(zI - A(\boldsymbol{\zeta}) - B(\boldsymbol{\zeta})K\big)^{-1} B_w(\boldsymbol{\zeta})\|_2 < \gamma,\ \forall \boldsymbol{\zeta} \in \Delta \tag{14}$$

if and only if there are real matrices $P = P^T > 0$, K and Z such that the following LMI system is satisfied

$$\begin{bmatrix} -P^{-1} & (A_i + B_i K) & 0 \\ (A_i + B_i K)^T & -P & (C_{z_i} + E_i K)^T \\ 0 & (C_{z_i} + E_i K) & -I \end{bmatrix} < 0 \tag{15}$$

$$\begin{bmatrix} P^{-1} & B_{w_i} \\ B_{w_i}^T & Z \end{bmatrix} > 0 \tag{16}$$

$$\mathrm{tr}(Z) < \gamma^2. \tag{17}$$

It is important to point out that this analysis result states that, to guarantee that matrix K satisfies (14) for all $\boldsymbol{\zeta} \in \Delta$, it is enough to ascertain that K satisfies (14) on the m points of the set Δ_0. The synthesis problem, i.e. that of finding a matrix $P = X^{-1}$ and controller K that verify (15-17), can be solved according to the following result.

Result 3. *The H_2 norm of the closed loop operator $\mathrm{T}_{\mathbf{zw}}(\boldsymbol{\zeta})$ is less than a positive number γ, that is, $\|\mathrm{T}_{\mathbf{zw}}(\boldsymbol{\zeta})\|_2 < \gamma$, with $\boldsymbol{\zeta} \in \Delta$ if a real symmetric matrix $X > 0$ ($X = P^{-1}$) and a real matrix Z exist such that*

$$(W_{1_i}^T A_i + W_{2_i}^T C_{z_i}) X (W_{1_i}^T A_i + W_{2_i}^T C_{z_i})^T - W_{1_i}^T X W_{1_i} - W_{2_i}^T W_{2_i} < 0 \tag{18}$$

$$\begin{bmatrix} X & B_{w_i} \\ B_{w_i}^T & Z \end{bmatrix} > 0 \tag{19}$$

$$\mathrm{tr}(Z) < \gamma^2, \tag{20}$$

where matrices $W_{1_i}^T$ and $W_{2_i}^T$ satisfy $\mathrm{im}[W_{1_i}^T \ W_{2_i}^T]^T = \ker[B_i^T \ E_i^T]$. Using the matrix solution X, the static state feedback gain K is then computed by solving the following LMI feasibility problem:

$$\begin{bmatrix} -X & A_i & 0 \\ A_i^T & -X^{-1} & C_{z_i}^T \\ 0 & C_{z_i} & -I \end{bmatrix} + \begin{bmatrix} B_i \\ 0 \\ E_i \end{bmatrix} K [0 \ I \ 0] + \begin{bmatrix} 0 \\ I \\ 0 \end{bmatrix} K^T [B_i^T \ 0 \ E_i^T] < 0. \tag{21}$$

This result can be easily proven by using the Projection Lemma,[5] followed by a decomposition of the null space matrices. Finally, the optimal solution for the discrete time H_2 control problem is approximated through the minimization of γ subject to Result 3.

B. Preview Controller Synthesis Technique

For augmented discrete time dynamic systems that include large preview intervals $p > 50$, the controller synthesis technique proposed in the last section leads to LMI optimization problems involving a large number of variables, which cannot easily be solved using the tools available today.

Going back to the preview control problem, consider the linear discrete time system (12). It is well known from the literature[1,2,12] that solutions for H_2 discrete time preview control problems can, in general, be decomposed into feedback and feedforward controllers by exploiting the particular structure of augmented preview dynamics. Building on these ideas, an alternative algorithm for computing the feedforward gain matrix is proposed.

To start with, consider an affine parameter-dependent system with the structure of (12), defined over a region Δ, with its m vertices in Δ_0. Restricting the parameter dependency to the state equation, let $\bar{A}_i$, $\bar{B}_i$, $\bar{B}_{w_i}$, $\bar{C}_z$, and $\bar{E}$ denote the state space matrices for the $i = 1, \ldots, m$ points in Δ_0. Assuming that $\mathbf{s}$ belongs to the disturbance vector $\mathbf{w}$, matrix $\bar{B}_{w_i}$ includes the preview input matrix $\bar{B}_s$. Consider also the central point of Δ, $\boldsymbol{\zeta}_o$, and the corresponding state space matrices $\bar{A}_o$, $\bar{B}_o$, and $\bar{B}_{w_o}$.

Partitioning matrices according to the augmented system structure, let $P = \begin{bmatrix} P_d & P_{ds} \\ P_{ds}^T & P_s \end{bmatrix}$, $Q = \bar{C}_z^T \bar{C}_z =$

$\begin{bmatrix} Q_d & Q_{ds} \\ Q_{ds}^T & Q_s \end{bmatrix}$, $R = \bar{E}^T\bar{E}$, and $K = [K_d\ ,\ K_s]$. Further assume that $\bar{C}_z^T\bar{E} = 0$. Applying Schur complements to the LMI (15), the following Lyapunov inequality is obtained:

$$(\bar{A}_i + \bar{B}_i K)^T P(\bar{A}_i + \bar{B}_i K) - P + (\bar{C}_z + \bar{E}K)^T(\bar{C}_z + \bar{E}K) < 0. \tag{22}$$

Simple manipulations show that the upper right block of (22) corresponds to a Lyapunov inequality of the form

$$(A_i + B_i K_d)^T P_d(A_i + B_i K_d) - P_d + Q_d + K_d^T R K_d < 0. \tag{23}$$

In view of these facts, the following result can be established.

Theorem 1. *Given a pair $(P_d,\, K_d)$, $P_d = P_d^T > 0$ that satisfies the conditions of Result 2, consider the matrix*

$$P_{ds} = [\tilde{A}_c^T P_d B_o,\, (\tilde{A}_c^2)^T P_d B_o,\, \cdots,\, (\tilde{A}_c^{p+1})^T P_d B_o] + [Q_1, \tilde{A}_c^T Q_1 + Q_2, ..., \sum_{j=1}^{p+1}(\tilde{A}_c^{p+1-j})^T Q_j], \tag{24}$$

where $\tilde{A}_c = A_o - B_o\left(B_o^T P_d B_o + R\right)^{-1} B_o^T P_d A_o$ and Q_j denotes the jth s-dimensional column block of matrix Q_{ds}, and the matrix P_s with entries

$$P_s(i,j) = \begin{cases} \Xi(i,j) & ,i \le s \ \vee\ j \le s \\ \Xi(i,j) + P_s(i-s, j-s) & ,i > s \ \wedge\ j > s \end{cases} \tag{25}$$

$$\Xi \quad = \quad H_o^T P_d H_o + H_o^T P_{ds} D + D^T P_{ds} H_o + Q_s - (P_d H_o + P_{ds} D)^T B_o (B_o^T P_d B_o + R)^{-1} B_o^T (P_d H_o + P_{ds} D).$$

Consider also the feedforward gain matrix

$$K_s = \left(B_o^T P_d B_o + R\right)^{-1} B_o^T \left(P_d H_o + P_{ds} D\right). \tag{26}$$

Then, the resulting closed-loop system is stable over the whole region Δ and the Lyapunov inequality for the central point verifies

$$(\bar{A}_o + \bar{B}_o K)^T P(\bar{A}_o + \bar{B}_o K) - P + (\bar{C}_z + \bar{E}K)^T(\bar{C}_z + \bar{E}K) = \begin{bmatrix} \Lambda & 0 \\ 0 & 0 \end{bmatrix} \le 0, \tag{27}$$

with $P = P^T > 0$.

Proof. Let $K = [K_d,\, K_s]$ be a stabilizing state feedback controller for system (12). Simple inspection of the structure of (12) shows that only K_d determines the stability of the closed-loop system. Since the pair (P_d, K_d) satisfies the conditions of Result 2, the stability of the closed-loop system over the whole region Δ is guaranteed.

To show that (27) is verified for the central point, consider the following expressions

$$L(P,K) \equiv (\bar{A}_o + \bar{B}_o K)^T P(\bar{A}_o + \bar{B}_o K) - P + (\bar{C}_z + \bar{E}K)^T(\bar{C}_z + \bar{E}K)$$

and

$$\tilde{L}(P) \equiv \bar{A}_o^T P \bar{A}_o - P - \bar{A}_o^T P^T \bar{B}_o \left(\bar{B}_o^T P \bar{B}_o + R\right)^{-1} \bar{B}_o^T P \bar{A}_o + Q,$$

such that $L(P,K) = 0$ and $\tilde{L}(P) = 0$ correspond to a Lyapunov equation and an algebraic Riccati equation (ARE), respectively. Assuming that $Q = \bar{C}_z^T \bar{C}_z$, $R = \bar{E}^T \bar{E}$, and $\bar{C}_z^T \bar{E} = 0$, it is straightforward to show that

$$L(P,K) = \tilde{L}(P) + (K - \tilde{K})^T \left(\bar{B}_o^T P \bar{B}_o + R\right)(K - \tilde{K}), \tag{28}$$

where $\tilde{K} = -\left(\bar{B}_o^T P \bar{B}_o + R\right)^{-1} \bar{B}_o^T P \bar{A}_o$. Using the structure of the augmented system matrices, (28) can be written as

$$\begin{bmatrix} \Lambda(P_d, K_d) & \Sigma(P,K) \\ \Sigma(P,K)^T & \Gamma(P,K) \end{bmatrix} = \begin{bmatrix} \tilde{\Lambda}(P_d) & \tilde{\Sigma}(P) \\ \tilde{\Sigma}(P)^T & \tilde{\Gamma}(P) \end{bmatrix} + \begin{bmatrix} K_d^T - \tilde{K}_d^T \\ K_s^T - \tilde{K}_s^T \end{bmatrix} \left(\bar{B}_o^T P \bar{B}_o + R\right) \left[K_d - \tilde{K}_d,\ K_s - \tilde{K}_s\right]. \tag{29}$$

where $\Lambda(P_d, K_d) < 0$ corresponds to the Lyapunov inequality (23) and $\tilde{\Lambda}(P_d) = 0$ takes the form of an ARE, both computed for the central system. Since K_s does not influence the stability of the closed loop system, one can impose that $K_s = \tilde{K}_s = (B_o^T P_d B_o + R)^{-1} B_o^T (P_d H_o + P_{ds} D)$, yielding $\Gamma = \tilde{\Gamma}$ and $\Sigma = \tilde{\Sigma}$.

From the hypothesis, it follows that $\Lambda(P_d, K_d) < 0$, which can be rewritten as $\tilde{\Lambda}(P_d) + (K_d - \tilde{K}_d)^T (B_o^T P_d B_o + R)(K_d - \tilde{K}_d) < 0$, and therefore $\tilde{\Lambda}(P_d) < 0$. Then, there exists a positive definite matrix δQ_d such that P_d is the unique positive definite solution to the ARE $\tilde{\Lambda}(P_d) + \delta Q_d = 0$. Defining a new ARE for the augmented system $\begin{bmatrix} \tilde{\Lambda}(P) + \delta Q_d & \tilde{\Sigma}(P) \\ \tilde{\Sigma}(P)^T & \tilde{\Gamma}(P) \end{bmatrix} = 0$, it can be shown that its unique positive definite solution is given by $P = \begin{bmatrix} P_d & P_{ds} \\ P_{ds}^T & P_s \end{bmatrix}$, where P_{ds}, and P_s satisfy equations (24) and (25), respectively. □

To evaluate the efficiency and validity of the method proposed for controller synthesis, a comparative analysis of the available methods was carried out. The results, presented in Table 1, include both the computation time and the closed-loop system's H_2 norm achieved by using the proposed method and by solving the set of LMI's for the augmented system. The results were computed for a forward flight trimming condition (linear body speed $V = 0.9$ ms^{-1}, zero angle of attack) and an increasing number of preview samples. Data presented in the table was obtained with a 3.00 GHz Intel Pentium 4 with 512MB of RAM running Matlab 6.5.0 on Microsoft Windows XP Professional.

The proposed method is indeed much faster than solving the LMI's for the augmented system, especially as the dimension of the preview vector increases, and achieves H_2 norm values very close to the ones given by the LMI optimization. Notice that, in practical terms, computation time for the optimal LMI-based method is no longer acceptable when the number of preview samples reaches twenty.

Table 1. Comparison of computation time and H_2 norms

	Proposed method		LMI-based method	
p	$\|.\|_2$	time[s]	$\|.\|_2$	time[s]
1	3.639	14.8	3.639	30.5
2	3.484	14.7	3.484	61.8
3	3.340	14.7	3.341	100.6
4	3.203	14.6	3.205	194.8
5	3.073	14.8	3.075	314.7
6	2.948	14.6	2.950	546.0
7	2.828	14.6	2.831	281.2
8	2.714	14.7	2.717	1312.6
9	2.605	14.7	2.609	1998.1
10	2.503	14.7	2.507	2810.1
15	2.090	14.7	?†	>3600
20	1.845	14.7	?†	>3600
30	1.692	14.9	?†	>3600
40	1.682	14.8	?†	>3600
50	1.677	14.9	?†	>3600
70	1.669	15.3	?†	>3600
100	1.668	16.3	?†	>3600

† Computation interrupted after one hour.

VI. Reference path

The preview-based tracking controller presented in the previous sections can be applied to terrain following for autonomous helicopters using different range sensing techniques. In this paper, a setup is considered wherein a Laser Range Scanner, mounted underneath the helicopter, scans the terrain along the vehicle's direction of forward flight, see Figure 8. As a result of this setup, a vector of reference points is available at all times and the full preview vector $\mathbf{x}_s(k)$ can be computed for every sampling instant. To consider this state vector in the tracking controller, it is assumed that for two consecutive sampling instants, the computed reference paths are very similar, so that the dynamics of $\mathbf{x}_s(k)$ can be approximated by (11).

The method adopted to build the reference path from measurement data is now presented. As shown in Figure 6, the laser readings, consisting of scanning angle and measured range, are transformed into 2-D terrain points, expressed in the body-fixed frame $\{B\}$. All the ensuing processing is performed with respect to this coordinate frame. The reconstruction points are interpolated by straight lines to approximate the terrain profile, while the actual reference path is obtained by "rolling" a circle along the reconstructed terrain profile and selecting the maximum for each x coordinate (see Figure 7). In this way, the reference path is guaranteed to keep a pre-specified safety distance from the terrain, defined as a perpendicular offset D_{off} to the reconstructed terrain profile.

As an example of the path building process, consider the case represented in Figure 8. It is clear that, for

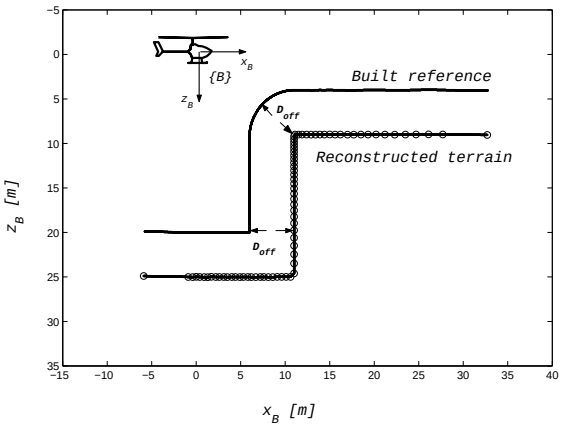

Figure 6. Reconstructed terrain profile and corresponding reference path.

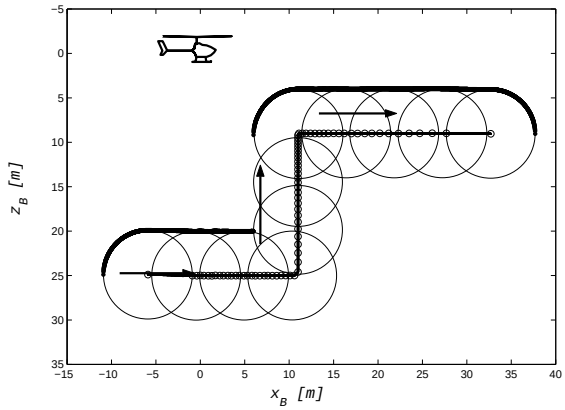

Figure 7. Rolling a circle of radius D_{off}, along the terrain profile.

high enough values of the scanning angle, the laser beam no longer hits any obstacle. For these readings, the laser is considered blind and a vertical wall shaped obstacle is assumed, for reasons of simplicity. The path building algorithm also handles occlusion problems, such as the one depicted in Figure 9, where the vehicle describes a climbing flight maneuver parallel to the wall and the sensor cannot acquire future information about the terrain profile ahead of this wall.

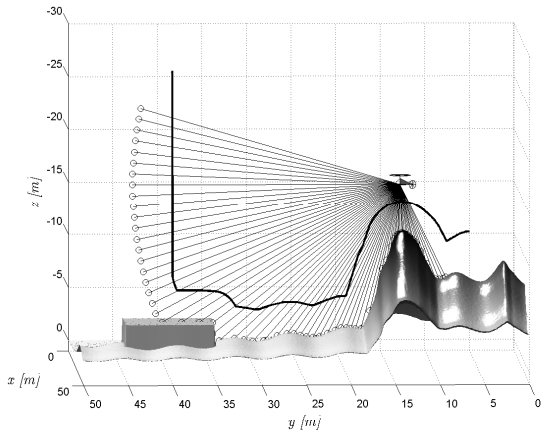

Figure 8. Example of terrain profile and corresponding reference path built from laser scan measurements.

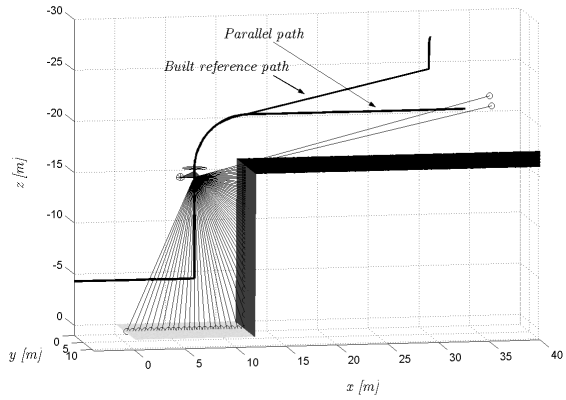

Figure 9. Step shaped terrain and actual reference path computed using out-of-range laser readings.

In this specific example, instead of ignoring the two laser readings that do not reach any obstacle, the algorithm uses them to capture the sudden change in the terrain and provide relevant preview information to the control system.

VII. Non-linear implementation

In the application presented here the vehicle is expected to follow the terrain moving along a vertical plane, with no sideslip, $\mathbf{v}_B = [u\ 0\ w]^T$. Under these assumptions, the angle of attack α and linear body speed $V = \|\mathbf{v}_B\|$ can be respectively approximated by $\alpha = \arctan\left(\frac{w}{u}\right)$, and $V = \sqrt{u^2 + w^2}$. During the controller design phase, the considered helicopter flight envelope was parameterized by $\boldsymbol{\zeta} = [V, \alpha]^T$ and partitioned into the 18 regions presented in Figure 10.

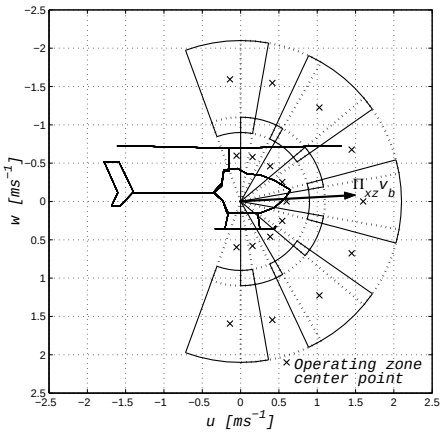

Figure 10. Operating regions parameterized by $\boldsymbol{\zeta} = [V, \alpha]^T$ and plotted in the velocity axes uOw.

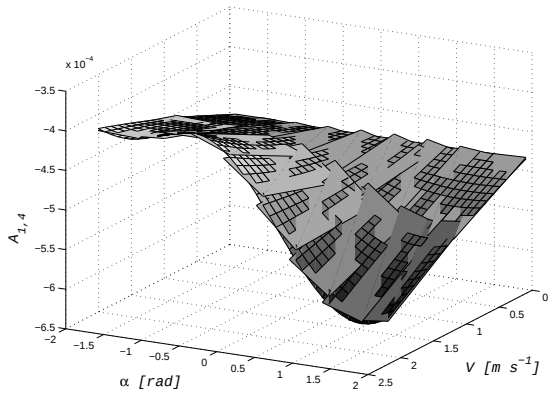

Figure 11. Surface and respective affine approximation obtained for element A_{14} as function of the velocity V and angle of attack α.

For each operating region, the elements of the discrete time state space matrices obtained from linearization of the error dynamics were approximated by affine functions of $\boldsymbol{\zeta}$ using a Least Squares Fitting. As an example, Figure 11 shows the surface obtained for element $(1, 4)$ of matrix $\bar{A}$ and the planes computed for the considered set of operating regions.

For a relatively dense grid of evaluated operating points, the affine approximation results in a maximum absolute error between matrix entries of less than 10% and a average absolute error of less than 2%.

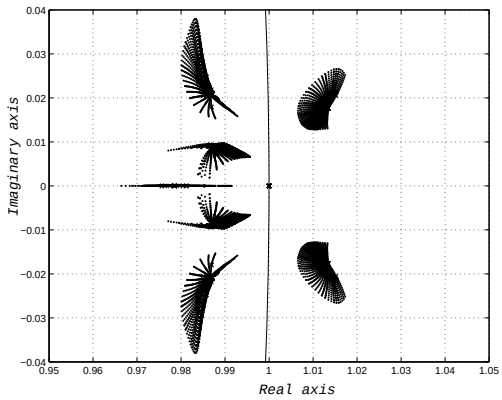

Figure 12. Dominant open-loop eigenvalues for the linearized systems.

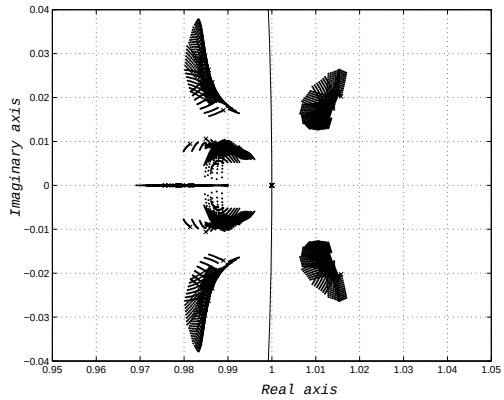

Figure 13. Dominant open-loop eigenvalues for the affine approximations.

To further validate the affine parameter-dependent approximation, Figures 12 and 13 display the dominant open-loop eigenvalues for the linearized systems and for the resulting affine approximations. It is important to stress that the eigenvalues have a similar variation with (V, α) and that the number of unstable eigenvalues remains constant.

A. Controller implementation

To implement the controller within the scope of gain scheduling control theory,[15] a state feedback matrix gain K_i was computed for each of the operating regions according to the technique presented in Section V. During the controller design phase, the regions were defined as overlaid to avoid fast switching between controllers, see Figure 10. The disturbance input matrix $\bar{B}_w$ was set to $\bar{B}_s$ and the state and control weight matrices $\bar{C}_z$ and $\bar{E}$ were set to

$$\bar{C}_z = \begin{bmatrix} \mathrm{diag}(\mathbf{c}_z) & \mathbf{0}_{15\times 3(p+1)} \\ \mathbf{0}_{4\times 15} & \mathbf{0}_{4\times 3(p+1)} \end{bmatrix}, \qquad \bar{E} = \begin{bmatrix} \mathbf{0}_{15\times 4} \\ 5I_{4\times 4} \end{bmatrix}, \tag{30}$$

where $\mathbf{c}_z = [0.5,\ 0.5,\ 0.5,\ 0.1,\ 0.1,\ 0.1,\ 1,\ 1,\ 0.01,\ 0.01,\ 0.1,\ 0.1,\ 0.1,\ 0.1,\ 0.1]^T$, yielding the performance vector

$$\mathbf{z} \;=\; [0.5\mathbf{v}_e^T,\ \ 0.1\boldsymbol{\omega}_e^T,\ \ \mathbf{d}_t^T,\ \ 0.01\phi_e,\ \ 0.01\theta_e,\ \ 0.1\psi_e,\ \ 0.1\mathbf{x}_i^T,\ \ 5.0\mathbf{u}^T]^T\,. \tag{31}$$

The final implementation scheme, presented in Figure 14, was achieved using the D-methodology described in Ref. 10. This methodology moves all integrators to the plant input, and adds differentiators where they are needed to preserve the transfer functions and the stability characteristics of the closed loop system. The D-methodology implementation has several important features that are worthwhile emphasizing: i) auto-trimming property - the controller automatically generates adequate trimming values for the actuation signals and for the state variables that are not required to track reference inputs; ii) the implementation of anti-windup schemes is straightforward, due to the placement of the integrators at the plant input.

VIII. Results

The following simulation results were obtained using the nonlinear dynamic model *SimModHeli*, which includes not only the rigid-body dynamics but also main rotor and Bell-Hiller stabilizing bar flapping dynamics. The model was parametrized for the Vario X-treme platform.

Figure 15 presents the entries of the preview feedforward control matrix K_s as a function of the preview time. In this case, a preview interval of 1 s, sampled at $T = 0.02$ s, is considered. It is clear that the weight of the preview signal decreases as the corresponding instant of time gets further ahead in the future, with negligible contributions above 0.8 s of preview time.

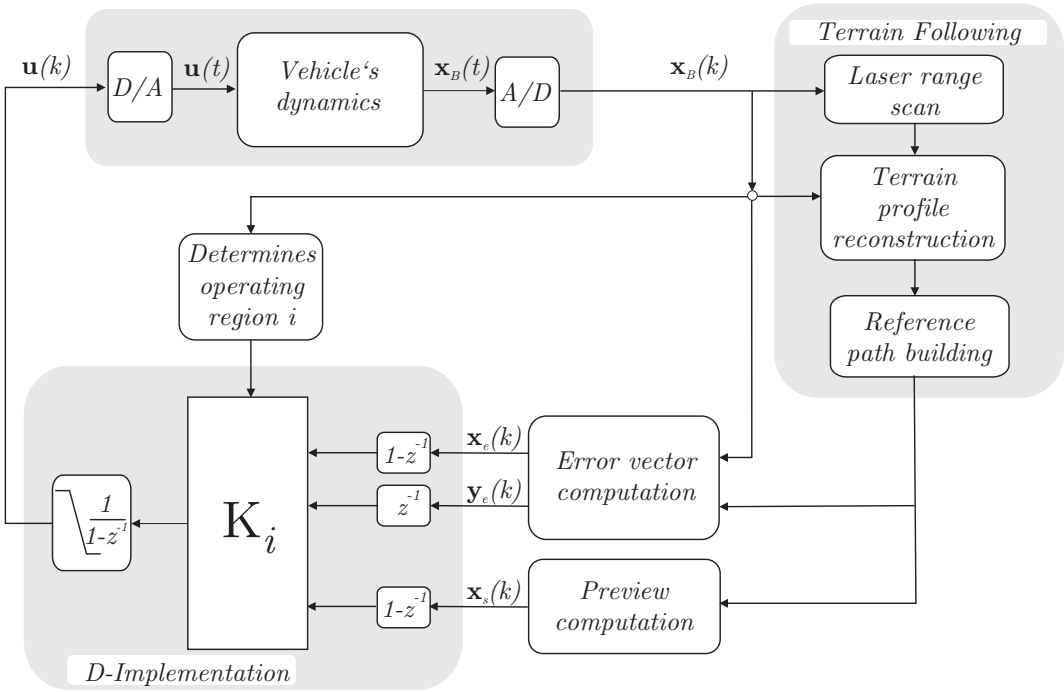

Figure 14. Implementation setup using gain scheduling and the D-methodology.

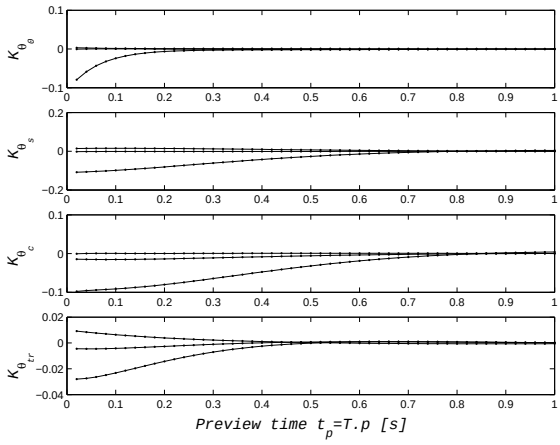

Figure 15. Evolution of the preview gains as a function of preview time.

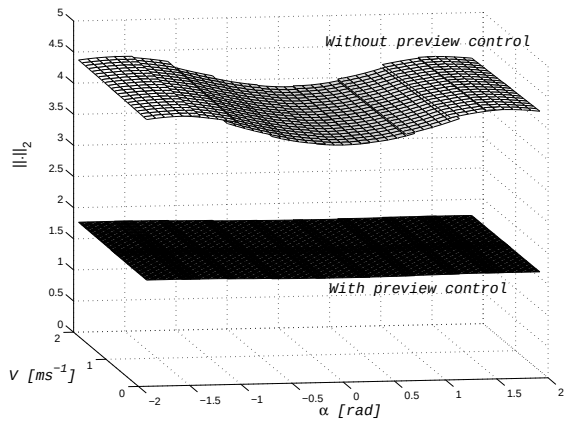

Figure 16. Closed-loop system's H_2 norm obtained with and without preview.

An additional tool used to assess the performance of the preview control scheme consists of comparing the H_2 norm of the linear closed-loop systems resulting from application of the control strategies with and without preview action. As shown in Figure 16, considering a mesh of operating points defined in V and α, the performance index for the preview-based solution is consistently below that of the traditional solution.

In Figure 17, the terrain following performance obtained with the proposed scheme is evaluated by varying the size of the preview vector and comparing the trajectories described by the vehicle, while following a step-shaped terrain profile. It can be observed that increasing the number preview samples, up to the value

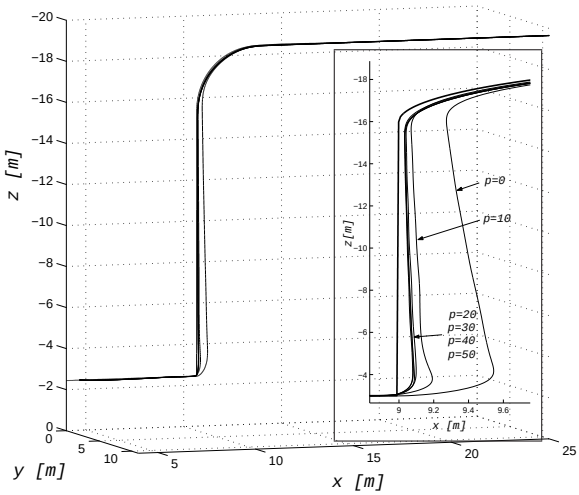

Figure 17. Terrain following performance obtained for different values of p, the size of the preview vector.

of 30, produces a clear improvement in performance. The fact that after a certain threshold no significant improvement is achieved is a natural result and corroborates the expected properties of the proposed method.

The time evolution of the error state vector $\mathbf{x}_e$ and actuation signals $\mathbf{u}$ corresponding to the $p = 50$ experiment is presented in Figures 18 and 19, respectively. It can be observed that signal activity, due to the preview action, clearly precedes transition points in the reference path. The vertical line marks the change in the reference path from forward to vertical flight. After each transition, both the state and input quickly converge to trimming values.

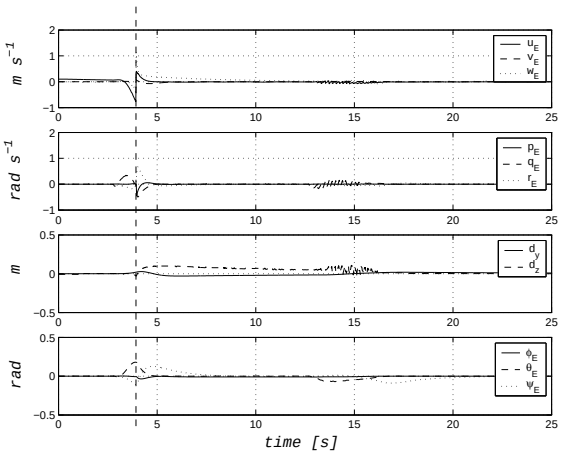

Figure 18. Time evolution of the error state $\mathbf{x}_e$.

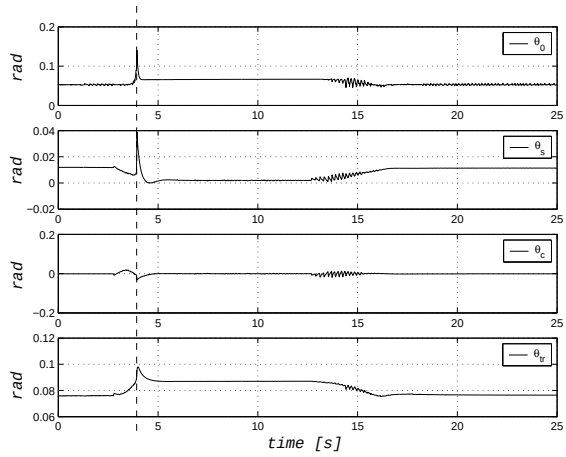

Figure 19. Time evolution of the actuation $\mathbf{u}$.

IX. Conclusions

The paper presented the design and performance evaluation of a laser based terrain following controller for rotorcraft. The technique described achieves good terrain following performance by taking into account, in the control law, the terrain characteristics ahead of the helicopter. Resorting to an H_2 controller design methodology for affine parameter-dependent systems, the technique presented exploits a new error space capable of naturally describing the particular dynamic characteristics of the helicopter in a suitable flight envelope. An alternative algorithm was proposed for computing the feed-forward gain matrix that avoids solving Linear Matrix Inequalities involving large numbers of unknowns. The resulting nonlinear controller was synthesized and implemented within the scope of gain-scheduling control theory, using a piecewise affine parameter-dependent model representation for the given set of operating regions. The effectiveness of the new control law was assessed in a MATLAB/Simulink simulation environment with a full nonlinear model of the Vario X-Treme helicopter. The quality of the results obtained clearly indicates that the methodology derived is suitable for the proposed application. Future work will include helicopter control close to the ground in the presence of strong wind action, extension of the presented technique to true three-dimensional terrain following using different sensors, and exploration of new error spaces along with new preview information inputs.

Acknowledgments

This work was supported in part by the FCT Programa Operacional da Sociedade de Informação (POSI) under the framework of the QCA III and by the POSI/SRI/41938/2001 ALTICOPTER project. The work of R. Cunha was supported by a PhD Student Scholarship, SFRH/BD/5034/2001, from the Portuguese FCT POCTI program.

References

[1]Tomizuka, M., "Optimum Linear Preview Control with Application to Vehicle Suspension-Revisited," *American Society of Mechanical Engineers - Journal of Dynamic Systems, Measurement, and Control*, Vol. 98, No. 3, 1976, pp. 309–315.

[2]Prokop, G. and Sharp, R. S., "Performance enhancement of limited bandwith active automotive suspensions by road preview," *Institution of Electrical Engineers Proceedings - Control Theory and Applications*, Vol. 142, No. 2, 1995, pp. 140–148.

[3]Takaba, K., "Robust servomechanism with preview action for polytopic uncertain systems," *International Journal of Robust Nonlinear Control*, Vol. 10, 2000, pp. 101–111.

[4]Hess, R. A. and Jung, Y. C., "An Application of Generalized Predictive Control to Rotorcraft Terrain-Following Flight," *IEEE Transactions on Systems, Man, and Cybernetics*, Vol. 19, No. 5, Sept. 1989, pp. 955–962.

[5]Ghaoui, L. E. and Niculescu, S. I., editors, *Advances in Linear Matrix Inequality Methods in Control*, Society for Industrial and Applied Mathematics, SIAM, Philadelphia, PA, 1999.

[6]Boyd, S., Ghaoui, L. E., Feron, E., and Balakrishnan, V., *Linear Matrix Inequalities in Systems and Control Theory*,

Society for Industrial and Applied Mathematics, SIAM, Philadelphia, PA, 1994.

[7]Cunha, R. and Silvestre, C., "A 3D Path-Following Velocity-Tracking Controller for Autonomous Vehicles," *16th IFAC World Congress*, Praha, Czech Republic, July 2005.

[8]Silvestre, C., Pascoal, A., and Kaminer, I., "On the Design of Gain-Scheduled Trajectory Tracking Controllers," *International Journal of Robust Nonlinear Control*, Vol. 12, 2002, pp. 797–839.

[9]Kaminer, I., Pascoal, A., Hallberg, E., and Silvestre, C., "Trajectory tracking for autonomous vehicles: An integrated approach to guidance and control," *AIAA Journal of Guidance, Control, and Dynamics*, Vol. 21, No. 1, 1998, pp. 29–38.

[10]Kaminer, I., Pascoal, A., Khargonekar, P., and Coleman, E., "A Velocity Algorithm for the Implementation of Gain-Scheduled Controllers," *Automatica*, Vol. 31, No. 8, 1995, pp. 1185–1191.

[11]Cunha, R. and Silvestre, C., "Dynamic Modeling and Stability Analysis of Model-Scale Helicopters with Bell-Hiller Stabilizing Bar," *AIAA Guidance, Navigation, and Control Conference*, Austin, TX, Aug. 2003.

[12]Libório, G., Paulino, N., Cunha, R., Silvestre, C., and Ribeiro, M. I., "Terrain following preview controller for model-scale helicopters," *Proceedings of ICAR 2003* - 11th *International Conference on Advanced Robotics*, Coimbra, Portugal, July 2003, pp. 1227–1232.

[13]Zhou, K., Doyle, J. C., and Glover, K., *Robust and Optimal Control*, Prentice Hall, Inc., Upper Saddle River, NJ, 1995.

[14]Scherer, C. and Weiland, S., *Lecture Notes on Linear Matrix Inequalities in Control*, Dutch Institute of Systems and Control, 2000.

[15]Rugh, W. and Shamma, J. S., "A Survey of Research on Gain-Scheduling," *Automatica*, Sept. 2000, pp. 261–268.